Flux-line cutting in granular high-temperature superconductors

F. Pérez-Rodríguez and A. Pérez-González
Instituto de Física, Universidad Autónoma de Puebla, Apartado Postal J-48, Puebla, Puebla 72570, Mexico

John R. Clem
Ames Laboratory and Department of Physics and Astronomy, Iowa State University, Ames, Iowa 50011

G. Gandolfini and M. A. R. LeBlanc
Department of Physics, University of Ottawa, Ottawa, Canada K1N 6N5
(Received 24 February 1997)

The magnetic response of granular high-temperature superconducting plates subjected to a dc-bias magnetic field and an increasing field perpendicular to it is studied both experimentally and theoretically. The theoretical model is based upon the double critical-state model, which considers not only flux transport but also flux-line cutting effects. Curves of magnetization for the system of grains decoupled by the applied magnetic field in sintered slabs of $YBa_2Cu_3O_{7-x}$ and $NdBa_2Cu_3O_{7-x}$ are analyzed. Good agreement between experimental results and theory is obtained. [S0163-1829(97)03730-2]

I. INTRODUCTION

At present there is great interest in studying the electromagnetic properties of the high-temperature superconductors.[1,2] These materials behave as irreversible type-II superconductors, and therefore many of their electromagnetic properties have been explained using approaches[3–11] based upon the Bean critical-state model.[12] However, when high-temperature superconductors are subjected to magnetic fields that change not only in magnitude but also in direction,[13–17] their electromagnetic response cannot be completely described by the usual critical-state model. This is because under those conditions, besides flux transport, the phenomenon of flux-line cutting[18,19] occurs. To take into account flux-line cutting effects, it is necessary to employ a more general approach, such as the double critical-state model.[20–25] This model makes use of two phenomenological parameters, namely, the transverse critical current density ($J_{c\perp}$) at the threshold of depinning and the longitudinal critical current density ($J_{c\parallel}$) at the threshold of flux-line cutting. These parameters depend on the material, temperature, and magnetic field. The double critical-state model has permitted the explanation of many intriguing experimental results in classical superconductors.[26–29] This model also has been applied to granular high-T_c superconductors to analyze flux-line cutting effects occurring in the weak-link regime of these materials.[14]

In the present work we shall study the occurrence of flux-line cutting in the magnetic response of granular high-temperature superconductors with sufficiently strong applied magnetic fields, so that deep penetration of magnetic flux into the decoupled grains occurs. As was shown in Ref. 13, in this situation flux-line cutting takes place inside the grains and affects the static magnetization curves. Here, we shall present experimental results and apply the double critical-state model to explain them. In Sec. II we describe the experiment. The theoretical model for studying the behavior of the electromagnetic fields inside the grains of high-temperature superconductors is presented in Sec. III. Theoretical and experimental results are compared in Sec. IV, and our conclusions are presented in Sec. V.

II. EXPERIMENT

Sintered slabs of $YBa_2Cu_3O_{7-x}$ (YBCO) and $NdBa_2Cu_3O_{7-x}$ (NdBCO) of thickness $x=0.16$ cm, width $y=1.2$ cm, and length $z=2.8$ cm (0.22, 1.2, and 2.4 cm), respectively, were prepared by Moreau at the Institut de Génie des Matériaux, Boucherville, Quebec, using standard prescriptions for preparing these high-T_c compounds starting with the oxide constituents.

Data on the flux expulsion upon field cooling from T_c to 77 K in various static fields and the ''standard'' magnetization curves along the length and width of these specimens have been reported by Gandolfini *et al.*[13] and aspects on their calibration discussed by LeBlanc.[30] Further details can be found in the M.Sc. thesis of G. Gandolfini.[31] These measurements indicate that the full intergrain (intragrain) penetration fields are ≈ 0.5 and 2 mT (12.8 and 14.5 mT) for the YBCO and NdBCO specimens, respectively, and the grains are effectively decoupled in fields greater than 5 mT.

A pickup coil embraces the specimen along its length and another along its width. Each pickup coil is series opposition connected to balancing coils that do not see the specimen but sense the corresponding applied magnetic field component of $\mathbf{H}_a$. Each set of orthogonal pickup coils feeds an electronic integrator/amplifier which drives the y axis of an XY_1Y_2 recorder. The x axis of the recorder is driven by a signal proportional to the component of the applied magnetic field $\mathbf{H}_a$ which is undergoing variation. A single layer of noninductively (i.e., bifilarly) wound manganin wire heater intimately embraces the specimen. The measurements reported in this paper begin with the specimen in the normal state in the selected field and terminate with the specimen again

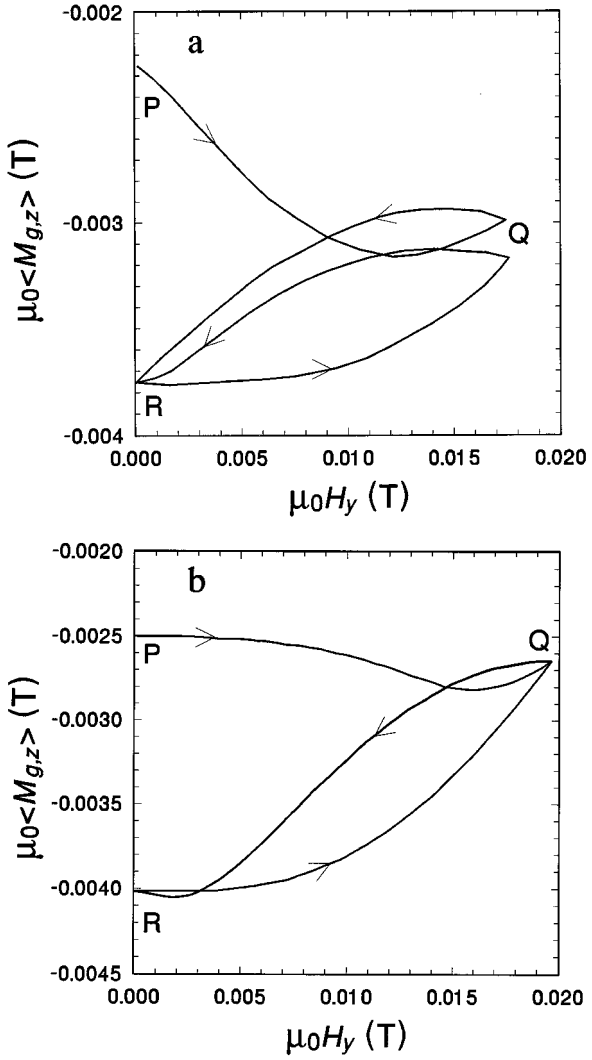

FIG. 1. (a) Evolution of the average magnetization of the grains $\langle M_{g,z}\rangle$ of the $YBa_2Cu_3O_{7-x}$ sample at 77 K while the component H_y of the applied magnetic field is impressed and cycled in the presence of the stationary bias field H_0. Here $\mu_0 H_0 = 10$ mT. (b) Theoretical curve (see text).

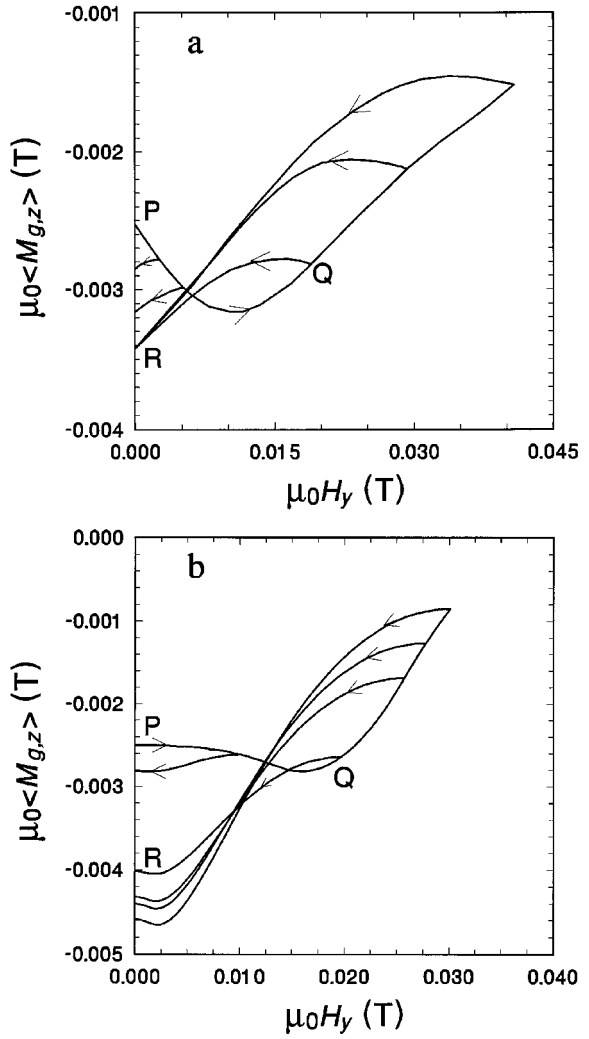

FIG. 2. (a) Response of the $NdBa_2Cu_3O_{7-x}$ specimen at 77 K to a first application and removal of H_y perpendicular to the static bias field $\mu_0 H_0 = 10$ mT. This figure illustrates the effect of increasing the amplitude H_y on the locus of $\langle M_{g,z}\rangle$ vs H_y. (b) Theoretical curve (see text).

driven to the normal state in the initial chosen field. Data curves that significantly fail to close because of electronic drift or drift in the static component of the initial field are rejected.

The longitudinal (z axis) magnetic field is generated by a 16-gauge copper wire solenoid of 18 cm length, 3.7 cm i.d., and 8.5 cm o.d. providing 20 mT/A. This solenoid is firmly secured inside an aluminum frame with a deep rectangular groove in which a 16-gauge copper wire coil is wound and provides the transverse (y axis) magnetic field of 3.7 mT/A. Transistorized battery-driven, hence ripple free, power sources supply the desired currents. The magnet coils and sample assembly are immersed in an open bath of liquid nitrogen.

Employing this experimental setup, we measured the magnetic moment of the decoupled grains of YBCO and NdBCO in the presence of the bias field H_0 parallel to the z axis upon slowly sweeping the perpendicular (y) component of the total applied field $\mathbf{H}_a = (0, H_y, H_0)$. The experimental results are shown in Figs. 1(a), 2(a), 3(a), and 4(a). The behavior of the observed hysteresis loops in the magnetization curves can be interpreted within the framework of the theoretical model constructed in the following section.

III. THEORY

Let us consider an infinite granular high-T_c superconducting plate with its surfaces at planes $x = 0$ and $x = d$. As in the experiment, the plate is assumed to be cooled through temperature T_c in the presence of an external magnetic field $\mathbf{H}_0$ parallel to the z axis. Afterward, a magnetic field in the y direction (H_y) is applied with slowly increasing magnitude. We shall study the case when the magnitude of the total field, H_a [$\mathbf{H}_a = (0, H_y, H_0)$], is large enough to suppress the intergranular supercurrents such that the grains inside the plate are decoupled. In our model we regard a superconducting plate formed by identical isotropic grains, having the shape of an infinite slab with thickness a (the characteristic size of the grains). It is noteworthy that the slab model for grains, in spite of its simplicity, has been successfully employed in several works (see, for instance, Refs. 4, 32, and 9)

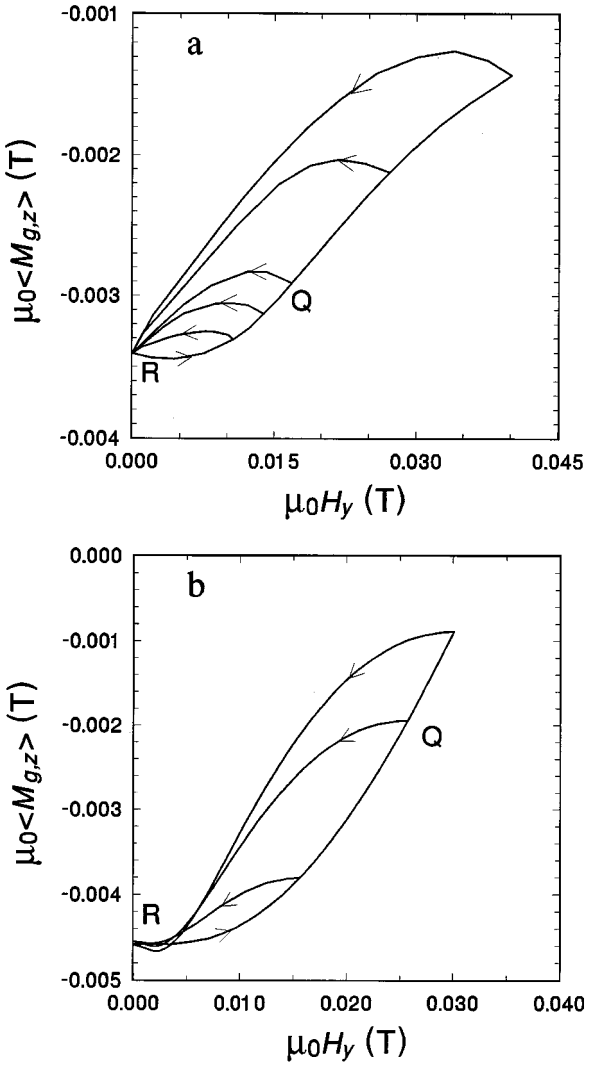

FIG. 3. (a) Illustration of the effect of different amplitudes of half cycles of H_y on the periodic response of $\langle M_{g,z} \rangle$ in the static bias field $\mu_0 H_0 = 10$ mT for the $NdBa_2Cu_3O_{7-x}$ specimen at 77 K. (b) Theoretical curves (see text).

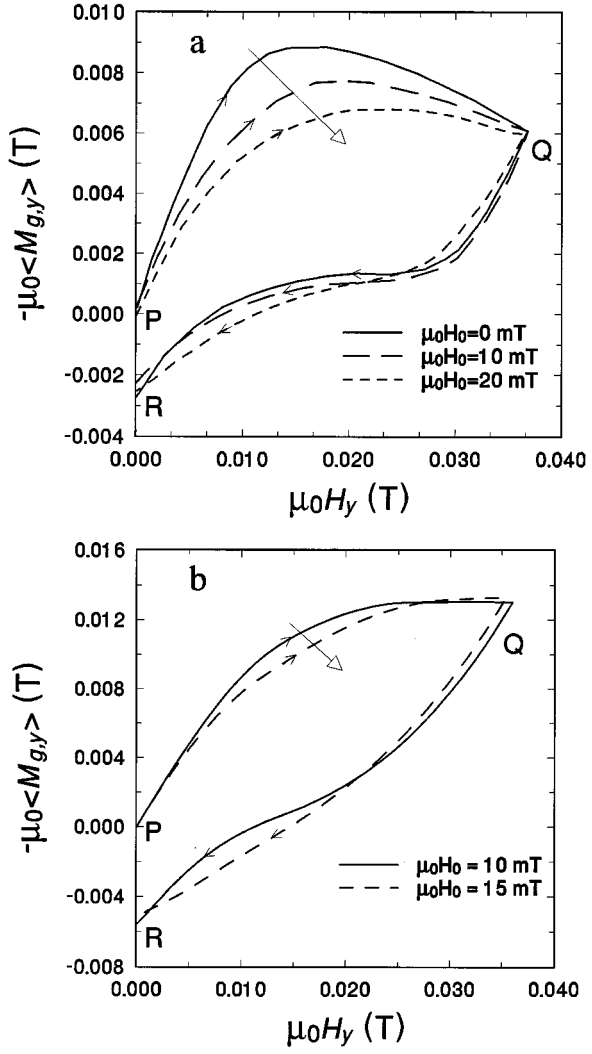

FIG. 4. (a) Illustration of the effect of the static bias field H_0 orthogonal to the varying magnetic field H_y on the average magnetization $\langle M_{g,y} \rangle$ for the $YBa_2Cu_3O_{7-x}$ sample. The static bias field $\mu_0 H_0 = 0$, 10, and 20 mT as indicated. (b) Theoretical curves for $\mu_0 H_0 = 10$ and 15 mT (see text).

for studying electromagnetic properties of high-T_c superconductors. In the space between the decoupled grains the magnetic induction obeys $\mathbf{B} = \mu_0 \mathbf{H}_a$, whereas in the grains $\mathbf{B} = \mu_0 \mathbf{H}$ and depends only on the x coordinate. It is convenient to express $\mathbf{B}(x)$ in the form

$$\mathbf{B}(x) = B(x)\hat{\alpha}(x), \tag{1}$$

where $B(x) = |\mathbf{B}(x)|$ and

$$\hat{\alpha}(x) = \hat{y}\ \sin\alpha(x) + \hat{z}\ \cos\alpha(x). \tag{2}$$

Here $\alpha(x)$ is the angle of $\mathbf{B}(x)$ with respect to the z axis. The intragranular current density $\mathbf{J}$ and the electric field $\mathbf{E}$ can be expressed in terms of their components parallel and perpendicular to $\mathbf{B}$:

$$\mathbf{J} = J_{\parallel}\hat{\alpha} + J_{\perp}\hat{\beta}, \tag{3}$$

$$\mathbf{E} = E_{\parallel}\hat{\alpha} + E_{\perp}\hat{\beta}, \tag{4}$$

where

$$\hat{\beta}(x) = \hat{\alpha}(x) \times \hat{x} = \hat{y}\ \cos\alpha(x) - \hat{z}\ \sin\alpha(x). \tag{5}$$

According to the assumed geometry, Maxwell's equations can be written as[21]

$$\frac{\partial B}{\partial x} = -\mu_0 J_{\perp}, \tag{6}$$

$$B\,\frac{\partial \alpha}{\partial x} = \mu_0 J_{\parallel}, \tag{7}$$

$$E_{\perp}\,\frac{\partial \alpha}{\partial x} - \frac{\partial E_{\parallel}}{\partial x} = -B\,\frac{\partial \alpha}{\partial t}, \tag{8}$$

$$\frac{\partial E_{\perp}}{\partial x} + E_{\parallel}\,\frac{\partial \alpha}{\partial x} = -\frac{\partial B}{\partial t}. \tag{9}$$

Here the displacement current is neglected.

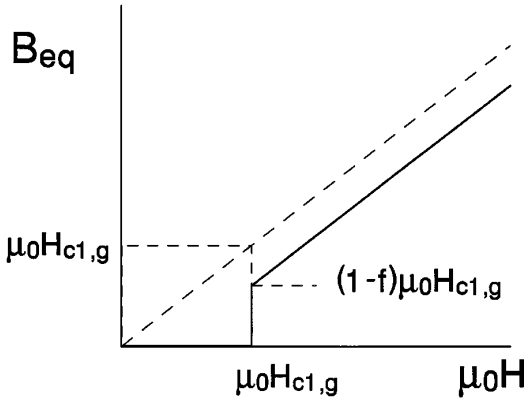

FIG. 5. Sketch of the model equilibrium $B_{\rm eq}$ vs H behavior used here.

We shall apply the constitutive relation between the electric field **E** and the current density **J** given by the double critical state model:[21–25]

$$E_\perp=\begin{cases}\rho_\perp[J_\perp-J_{c\perp}(B)], & J_\perp>J_{c\perp},\\ 0, & 0\leqslant J_\perp\leqslant J_{c\perp},\end{cases} \tag{10}$$

and

$$E_\parallel=\begin{cases}\rho_\parallel[J_\parallel-J_{c\parallel}(B)], & J_\parallel>J_{c\parallel},\\ 0, & 0\leqslant J_\parallel\leqslant J_{c\parallel},\end{cases} \tag{11}$$

where $E_\perp(-J_\perp)=-E_\perp(J_\perp)$, $E_\parallel(-J_\parallel)=-E_\parallel(J_\parallel)$, $\rho_\perp$ and $\rho_\parallel$ are effective flux-flow and flux-line-cutting resistivities of the grains, and $J_{c\parallel}$ and $J_{c\perp}$ are magnitudes of the critical current densities parallel and perpendicular to **B**.

In the experiment (Sec. II) the magnitude of the applied magnetic field has values larger than the first critical field of the grains $H_{c1,g}$, which is of the order of a few mT for $YBa_2Cu_3O_{7-x}$ and $NdBa_2Cu_3O_{7-x}$, i.e.,

$$H_a>H_{c1,g}. \tag{12}$$

In this case the boundary conditions for the system of equations (6)–(11) are given by the magnitude of the equilibrium magnetic induction at grain surfaces

$$B(x_i)=B(x_i+a)=B_{\rm eq}(H_a), \tag{13}$$

where x_i and x_i+a denote the positions of the surfaces of the ith slablike grain. The function $B_{\rm eq}(H)$ in Eq. (13) can be approximated by using the formula[33,34]

$$B_{\rm eq}=\mu_0 H-f\mu_0 H_{c1,g}. \tag{14}$$

Here the parameter f $(0<f<1)$ is a constant factor to approximate the sharp rise of the equilibrium magnetic induction $B_{\rm eq}$ near $H_{c1,g}$ (see Fig. 5). In addition, the boundary conditions for the angle α of the magnetic induction are

$$\tan\alpha(x_i)=\tan\alpha(x_i+a)=\frac{H_y}{H_0}. \tag{15}$$

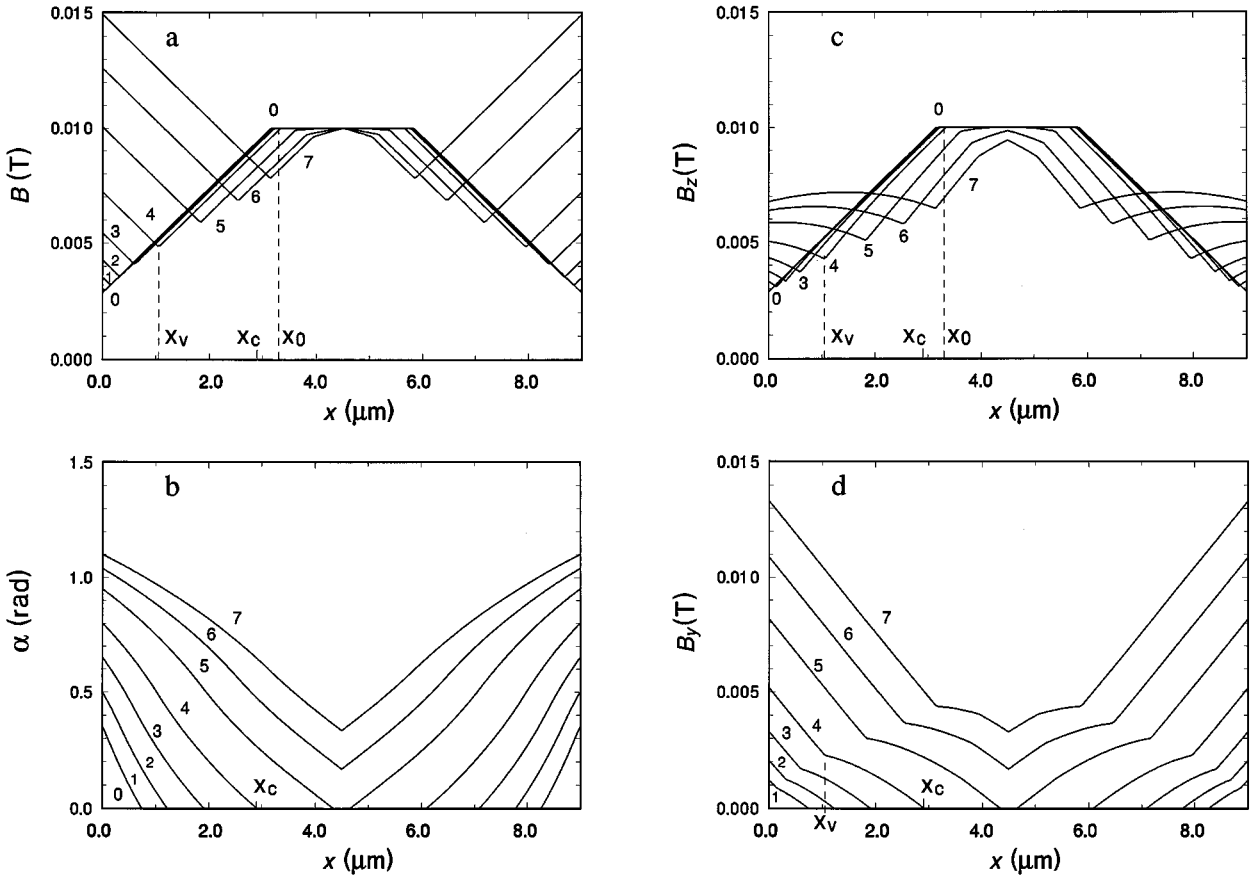

FIG. 6. Families of (a) B, (b) α, (c) B_z, and (d) B_y profiles for the first half cycle of H_y as discussed in Sec. IV.

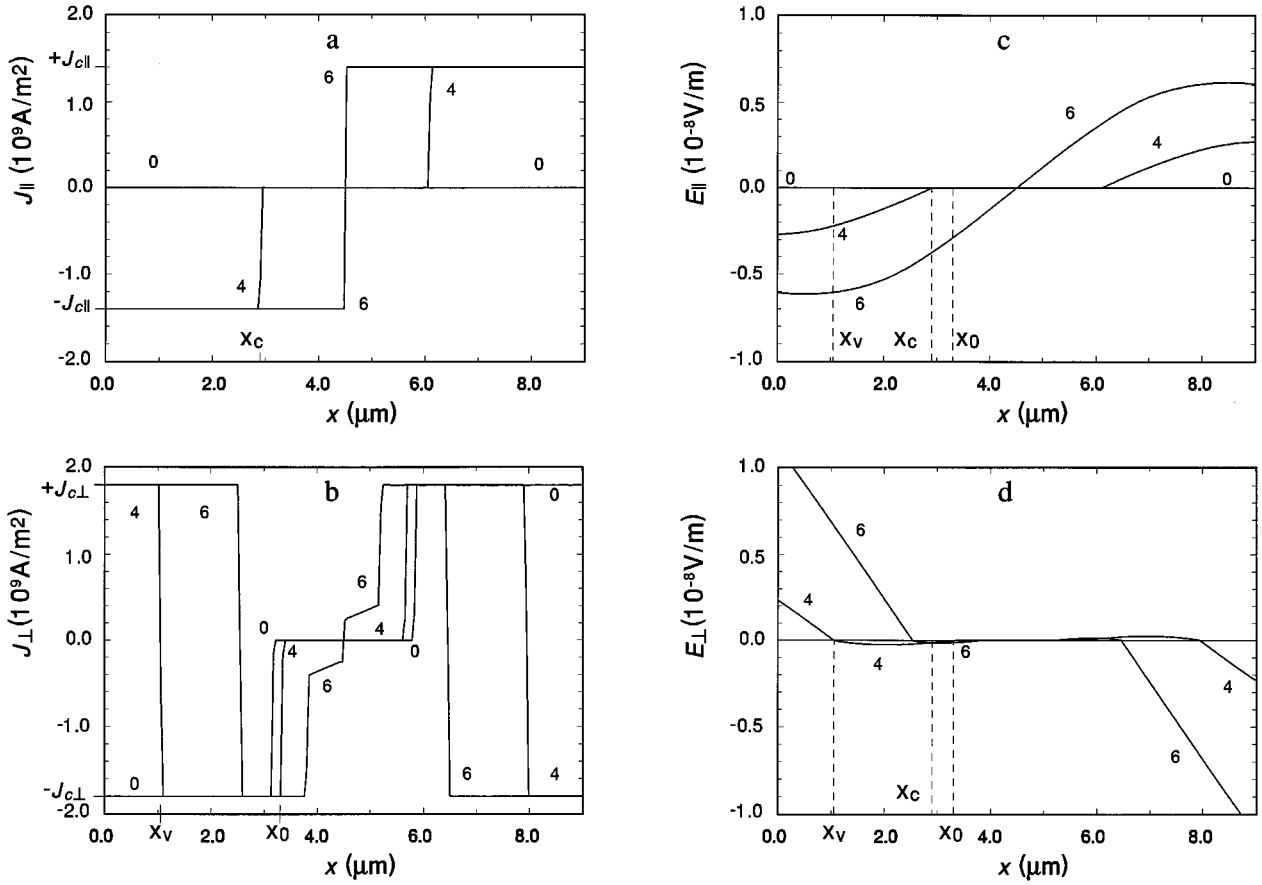

FIG. 7. Families of (a) $J_\parallel$, (b) $J_\perp$, (c) $E_\parallel$, and (d) $E_\perp$ profiles for the first half cycle of H_y as discussed in Sec. IV.

When the inequality Eq. (12) holds, the process of field cooling in a high-temperature superconductor is characterized by a fractional Meissner effect,[35] and, because of pinning forces acting on vortices, some portion of the magnetic flux inside the grains is trapped. Another factor that also affects the magnetic-flux expulsion is the rate of cooling,[36] especially when the strength of pinning is strong.[34] These factors should be taken into account in determining the spatial distribution of the magnetic induction after field cooling. Here, for simplicity, we assume that this distribution is the same inside all the grains. Hence, the average magnetization of the superconducting plate

$$\langle \mathbf{M}_{\rm pl} \rangle = \frac{1}{\mu_0 d} \int_0^d \mathbf{B}(x)dx - \mathbf{H}_a , \tag{16}$$

is related to the average magnetization of a grain,

$$\langle \mathbf{M}_g \rangle = \frac{1}{\mu_0 a} \int_{x_i}^{x_i+a} \mathbf{B}(x)dx - \mathbf{H}_a , \tag{17}$$

by the expression

$$\langle \mathbf{M}_{\rm pl} \rangle = f_g \langle \mathbf{M}_g \rangle , \tag{18}$$

where f_g is the fraction of the volume occupied by the grains. The experimental results shown in Sec. II correspond to the magnetization of the decoupled grains because of the calibration used. Therefore we shall calculate directly the magnetization of a single grain $\langle \mathbf{M}_g \rangle$ (17) with $x_i = 0$.

IV. RESULTS AND DISCUSSION

Figures 1(b), 2(b), 3(b), and 4(b) show theoretical graphs for the average magnetization of the decoupled grains in $YBa_2Cu_3O_{7-x}$ and $NdBa_2Cu_3O_{7-x}$ superconducting plates. In the calculation of the curves, first we determined the profile $B(x)$ after field cooling (curve 0 in Fig. 6) by applying the critical state model and using a value for the critical current density $J_{c\perp}(T)$ equal to that at the final temperature $T < T_c$. This approximation turns out to be good even if the pinning is quite strong, i.e., $J_{c\perp} a > H_0$.[34] The parameters used are $a = 9\ \mu$m, $J_{c\perp} = 1.8 \times 10^9$ A/m^2, and $J_{c\parallel} = 1.4 \times 10^9$ A/m^2; that is, the critical-current densities are assumed to be independent of B. Finally, the parameter $f\mu_0 H_{c1,g}$ in Eq. (14) is found from the experimental measurement for $\mu_0 \langle M_{g,z} \rangle$ after field cooling (at $H_y = 0$). Here, we chose $\mu_0 \langle M_{g,z} \rangle = -2.5$ mT, as in the case of the $NdBa_2Cu_3O_{7-x}$ sample, which has a magnetization slightly lower than the corresponding value (≈ -2.3 mT) for the magnetization $\langle M_{g,z} \rangle$ of the $YBa_2Cu_3O_{7-x}$ specimen.

The evolution of $\langle M_{g,z} \rangle$ for $H_0 = 10$ mT, as the y component of the external field is increased, is observed in Fig. 1. A characteristic feature of the manifestation of flux-line cutting is the initial decrease of the magnetization $\langle M_{g,z}(H_y) \rangle$. For sufficiently large values of H_y, the z component of the magnetization first reaches a minimum and later increases (curve $P \rightarrow Q$ in Fig. 1). The return of H_y to 0 produces again a decrease in the magnetization (curve $Q \rightarrow R$). The value of $\langle M_{g,z} \rangle$ at point R turns out to be lower than at the initial

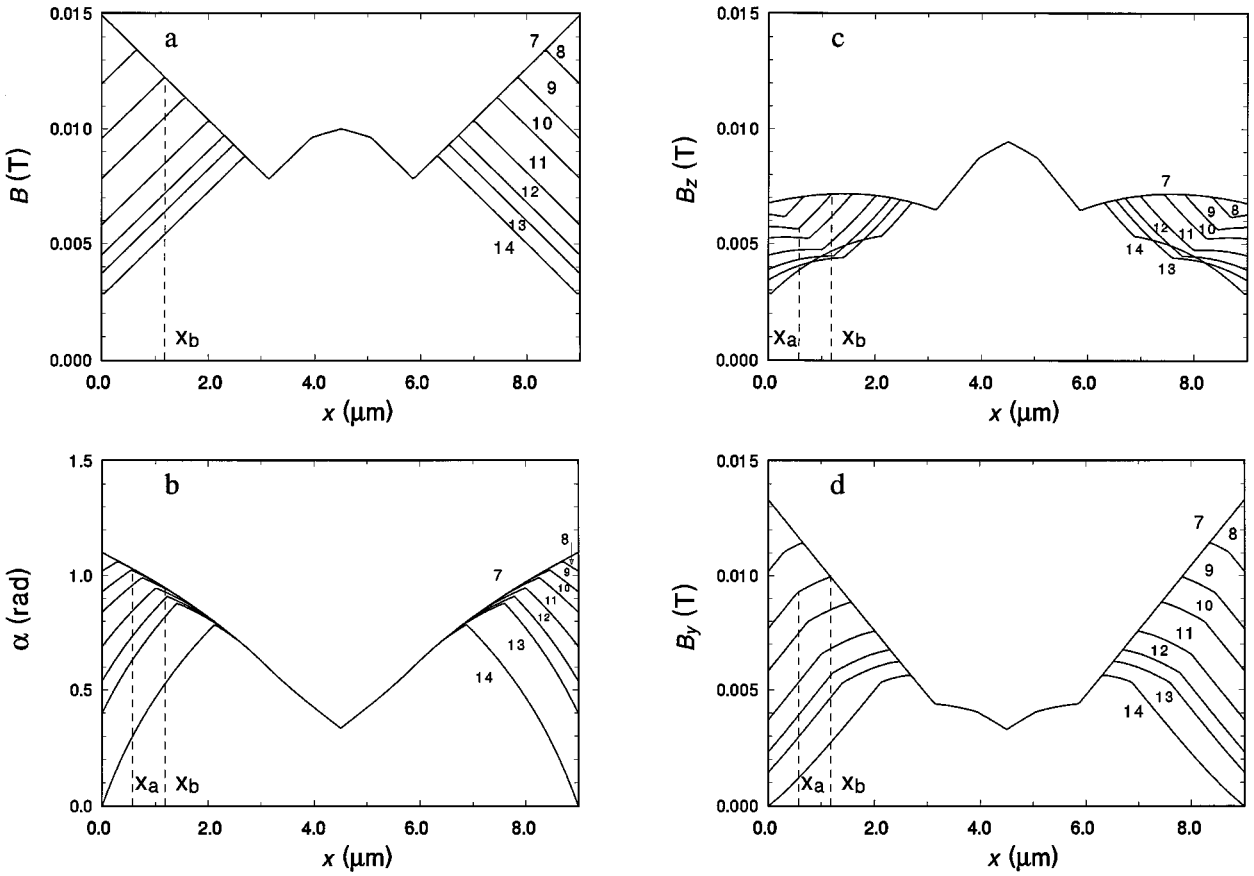

FIG. 8. Families of (a) B, (b) α, (c) B_z, and (d) B_y profiles for the second half cycle of H_y as discussed in Sec. IV.

point P (see Fig. 1). In a second cycle of H_y (curves $R\rightarrow Q$ and $Q\rightarrow R$), a hysteresis loop in the magnetization is generated.

Curves of the magnetization parallel to $\mathbf{H}_0$ for different initial ($P\rightarrow Q\rightarrow R$) and secondary ($R\rightarrow Q\rightarrow R$) cycles are presented in Figs. 2 and 3, respectively. The theoretical curves agree qualitatively with the experimental ones. Note that the best agreement between theory and experiment is observed in the range of large values of H_y.

The y component of the magnetization (see Fig. 4) as a function of H_y has a similar form as in the case $H_0=0$. The effect of flux line cutting can be best observed by comparing curves for different applied fields H_0. As is seen, the evolution of the magnetization $\langle M_{g,y}(H_y)\rangle$ with increasing H_0 [Fig. 4(a)] is reproduced by our theoretical results [Fig. 4(b)].

In Figs. 6 and 7 we present the evolution of the fields $B(x)$, $\alpha(x)$, $B_z(x)$, $B_y(x)$, $J_{\parallel}(x)$, $J_{\perp}(x)$, $E_{\parallel}$, and $E_{\perp}(x)$ in a slablike grain as the external magnetic field H_y is increased ($P\rightarrow Q$). These graphs were calculated with the same parameters as in Figs. 1(b) and 2(b). The spatial distribution of the magnetic induction after field cooling is given by curves labeled with 0. This initial distribution is typical for the case of strong pinning when a large portion of the magnetic flux is trapped inside the superconducting grains.[34] The slopes of $B(x)$ and $B_z(x)$ near grain boundaries are given by the critical-current density $J_{c\perp}$ [$\partial B(x)/\partial x=\pm\mu_0 J_{c\perp}$]. The initial distribution of current density is presented in Fig. 7(b), curve 0.

When the y component of the magnetic field is switched on, the penetration of additional magnetic flux into the grains occurs, being obstructed by pinning forces. As a consequence, the magnetic induction $B(x)$ increases near grain boundaries [see curves 1–7 in Fig. 6(a)], but decreases inside the grains because of flux-line cutting. Thus, two V-shaped minima in $B(x)$ appear at x_v and $a-x_v$. As is seen in Fig. 7(b), in the region between these minima and the boundaries the current density $J_{c\perp}(x)$ changed its initial sign. The new sense of the current corresponds to the sign of the induced electric field $E_{\perp}$ [Fig. 7(d)]. Because of the change in direction of the external magnetic field $\mathbf{H}_a$, the angle distribution $\alpha(x)$ also is altered [Fig. 6(b)]. For relatively small values of H_y (curves 1–5) the angle α decreases from its surface value [$\alpha(0)=\alpha(a)$] to zero at points $x_c(x_v<x_c<a/2)$ and $a-x_c$. This monotonic inward decrease of $\alpha(x)$ depends on both the parallel critical-current density $J_{c\parallel}$ and the magnitude of the magnetic induction B [see Eq. (7)]. In the zones $0<x<x_c$ and $a-x_c<x<a$, both perpendicular and parallel components of the electric field $\mathbf{E}$ are different from zero [Figs. 7(c) and 7(d)]. These zones are called CT zones because flux-line cutting and transport occur.[21,23] As is seen in Fig. 6, in the subintervals $0<x<x_v$ and $a-x_v<x<a$ of these CT zones the transport is toward the interior of the grains, whereas in the subintervals $x_v<x<x_c$ and $a-x_c<x<a-x_v$ the transport is from the center of the grain outwards. The change of sign of the electric field $E_{\perp}$ [Fig. 7(d)] is connected to the change of sense of the transport. In the zones $x_c<x<x_0$ and $a-x_0<x<a-x_c$ [Figs. 7(c) and 7(d), curves 4] it turns out that $E_{\parallel}=0$ and $E_{\perp}\neq 0$. These zones are T zones because only transport occurs. The unaltered zone of

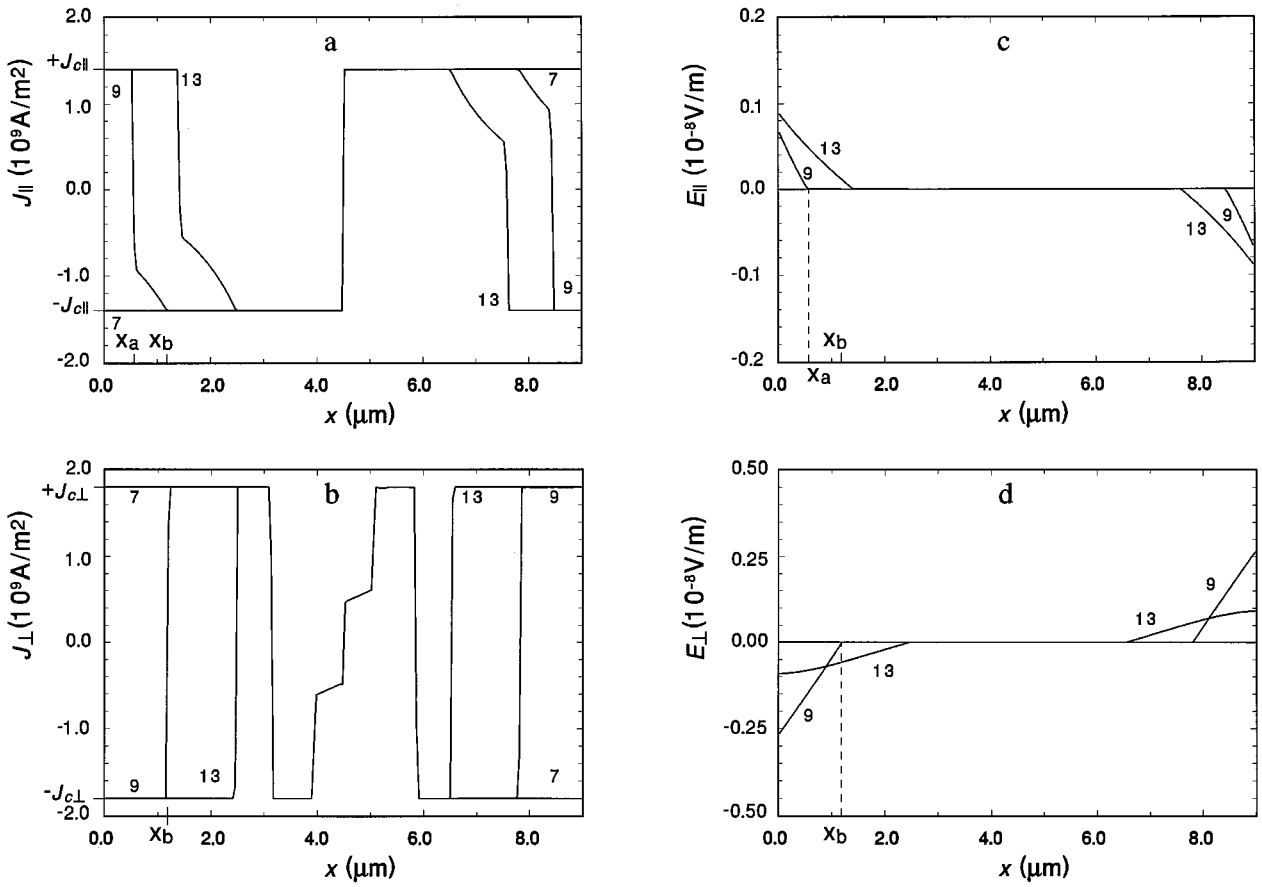

FIG. 9. Families of (a) $J_\parallel$, (b) $J_\perp$, (c) $E_\parallel$, and (d) $E_\perp$ profiles for the second half cycle of H_y as discussed in Sec. IV.

curve 4, $x_0<x<a-x_0$ is named the 0 zone. Moreover, the resulting profiles of $B(x)$ also possess C zones, where only flux-line cutting occurs ($E_\perp=0$ and $E_\parallel\neq 0$) and the derivative $|\partial B/\partial x|$ and perpendicular current density $|J_\perp|$ are equal to or smaller than their corresponding critical values [see curves 6 in Figs. 7(a), 7(b), 7(c), and 7(d), where the C zone straddles the middle of the grain]. If H_y is sufficiently large, the direction of the magnetic induction is modified in the entire grain; i.e., $x_c=a/2$ [Fig. 6(b), curves 6,7]. In this case, C and CT zones occur, but the 0 and T zones disappear.

The components $B_z=B\cos\alpha$ [Fig. 6(c)] and $B_y=B\sin\alpha$ [Fig. 6(d)] also have a complex behavior as H_y is varied. The increment of B_z at the grain surfaces is interesting since the field $H_0\|\hat{z}$ is fixed. This increment is determined by the function $B_{\rm eq}(H)$. So, according to our model [Eq. (14)],

$$B_z(0)=B_{\rm eq}\cos\alpha(0)=\mu_0 H_0-f\mu_0 H_{c1,g}\cos\alpha(0). \quad (19)$$

From this expression we see that the term with the parameter f increases with $\alpha(0)$. In spite of this, the decrease of B and B_z in the inner zones (CT and T) dominates the magnetization. For this reason, the average magnetization $\langle M_{g,z}\rangle=\langle B_z\rangle/\mu_0-H_0$ decreases with H_y (curves $P\rightarrow Q$ in Figs. 1 and 2). On the other hand, as is seen in Fig. 6(d) with increasing the external magnetic field H_y, the y component of the magnetic induction increases at the grain surfaces but is smaller inside the grains. This behavior of $B_y(x)$ leads to a negative average magnetization $\langle M_{g,y}\rangle=\langle B_y\rangle/\mu_0-H_y$ whose magnitude increases as the magnetic field H_y is applied (curves $P\rightarrow Q$ in Fig. 4).

Now, let us analyze the behavior of the fields inside the grains in the second half of the initial cycle of H_y (curves $Q\rightarrow R$ in Figs. 1 and 2). In Figs. 8 and 9 we show families of theoretical curves for $B(x)$, $\alpha(x)$, $B_z(x)$, $B_y(x)$, $J_\parallel(x)$, $J_\perp(x)$, $E_\parallel$, and $E_\perp(x)$. The initial profile of the magnetic induction is labeled as curve 7 in Fig. 8 and corresponds to the spatial distribution of $\mathbf{B}(x)$ at the maximum chosen value of H_y. With diminution of the applied magnetic field H_y, magnetic flux is expelled from the grains. Because of pinning, the magnetic induction $B(x)$ is reduced only near the surface, i.e., in the intervals $0<x<x_b$ and $a-x_b<x<a$ [see curves 8–14 in Fig. 8(a)]. The derivative $\partial B/\partial x$ and the current density $J_\perp$ [Fig. 9(b)] in these intervals take their critical values. In addition, the angle $\alpha(x)$ is reduced in the altered zones, and break points appear in its profile at points $x_a(x_a<x_b)$ and $a-x_a$ [Fig. 8(b)]. The regions $0<x<x_a$ and $a-x_a<x<a$ are CT zones since $E_\perp\neq 0$ and $E_\parallel\neq 0$ (Fig. 9). From Figs. 8(b) and 9(a) we see that in the zones $x_a<x<x_b$ and $a-x_b<x<a-x_a$ the profiles $\alpha(x)$ are subcritical; i.e., the magnitude of the corresponding parallel current density [Eq. (7)] is smaller than $J_{c\parallel}$. These zones are of type T (Refs. 21, 23) because transport occurs but flux-line cutting does not ($E_\perp\neq 0$, $E_\parallel\approx 0$, see Figs. 9(c) and 9(d)]. Finally, the region $x_b<x<a-x_b$ is unaltered (0 zone), but here the behavior of the magnetic induction is the same as in the beginning of the second half of the initial H_y cycle ($P\rightarrow Q\rightarrow R$).

The components of the magnetic induction $B_z(x)$ [Fig. 8(c)] and $B_y(x)$ [Fig. 8(d)] show a considerable decrease in the second half of the initial cycle of H_y. Nevertheless, the average magnetization $\langle M_{g,z}(H_y)\rangle$ decreases, whereas $\langle M_{g,y}(H_y)\rangle$ increases from the point Q to the point R [see Figs. 1(b), 2(b), 4(b)].

The behavior of the fields in the secondary cycles of H_y, $R\rightarrow Q\rightarrow R$, is similar to the cycle $P\rightarrow Q\rightarrow R$. However, now the initial profile of $\mathbf{B}(x)$ for the secondary cycles is given by the curves 14 of Fig. 8. In the cycles $R\rightarrow Q\rightarrow R$, as was noted above, the increase of $H_y(R\rightarrow Q)$ leads to an increase of the average magnetization parallel to H_0, since in this situation the transport of magnetic flux into the grains turns out to be dominant. Finally, we should note that in some cycles the maximum value of H_y is quite large (see Figs. 3 and 4). In such a case all the migrating points x_0, x_c, x_v, x_b, and x_a can reach the middle of the grain, $x=a/2$.

V. CONCLUSIONS

We have studied the magnetic response of granular high-temperature superconductors ($YBa_2Cu_3O_{7-x}$ and $NdBa_2Cu_3O_{7-x}$) in the presence of a magnetic field $\mathbf{H}_a=(0,H_y,H_0)$ by sweeping one of the components H_y. Because of the relatively large magnitude of the applied field, the grains are electrically decoupled. As is shown, under these conditions the phenomenon of flux-line cutting occurs inside the grains of a granular high-temperature superconductor and produces characteristic hysteresis loops in the magnetization curves. Using the double critical-state model, we could reproduce the main features of the experimental curves. The model also permits a detailed examination of the behavior of the magnetic induction inside the grains and the identification of the zones where flux transport and/or flux-line cutting occur.

ACKNOWLEDGMENTS

Ames Laboratory is operated for the U.S. Department of Energy by Iowa State University under Contract No. W-7405-Eng-82. This research was supported by the Director of Energy Research, Office of Basic Energy Sciences. F.P.-R. thanks Fundación México-Estados Unidos para la Ciencia, Academia de Investigación Científica (México) and International Institute of Theoretical and Applied Physics, Iowa State University, for their financial support.

[1] E. H. Brandt, Rep. Prog. Phys. **58**, 1465 (1995).
[2] D. B. Tanner and T. Timusk, in *Physical Properties of High Temperature Superconductors III*, edited by D. M. Ginsberg (World Scientific, Singapore, 1992), Chap. 5.
[3] H. Dersch and G. Blatter, Phys. Rev. B **38**, 11 391 (1988).
[4] J. R. Clem, Physica C **153-155**, 50 (1988).
[5] R. L. Peterson, Phys. Rev. B **40**, 2678 (1989).
[6] E. M. Gyorgy, R. B. van Dover, K. A. Jackson, L. F. Schneemeyer, and J. V. Waszczak, Appl. Phys. Lett. **55**, 283 (1989).
[7] D. D. Stancil, T. E. Schlesinger, A. K. Stamper, and D. Wong, J. Appl. Phys. **64**, 5899 (1988).
[8] M. Xu, D. Shi, and R. F. Fox, Phys. Rev. B **42**, 10 773 (1990).
[9] L. M. Fisher, I. F. Voloshin, N. M. Makarov, V. A. Yampol'skii, E. López-Cruz, and F. Pérez-Rodríguez, J. Appl. Phys. **75**, 7414 (1994).
[10] P. Fournier, M. Aubin, and M. A. R. LeBlanc, Phys. Rev. B **50**, 9548 (1994).
[11] X. Xu, J. Fang, X. Cao, and K. Li, Solid State Commun. **93**, 291 (1995).
[12] C. P. Bean, Phys. Rev. Lett. **8**, 250 (1962).
[13] G. Gandolfini, M. A. R. LeBlanc, and J. Sekerka, Cryogenics **29**, 373 (1989).
[14] M. A. R. LeBlanc, S. Çelebi, S. X. Wang, and V. Plecháčêk, Phys. Rev. Lett. **71**, 3367 (1993).
[15] L. M. Fisher, A. V. Kalinov, I. F. Voloshin, I. V. Baltaga, K. V. Il'enko, and V. A. Yampol'skii, Solid State Commun. **97**, 833 (1996).
[16] L. M. Fisher, A. V. Kalinov, J. Mirkovic, I. F. Voloshin, S. A. Zver'kov, A. Bondarenko, M. Obolenskii, V. A. Yampol'skii, and R. L. Snyder, Appl. Supercond. **2**, 639 (1994).
[17] K. V. Bhagwat, S. V. Nair, and P. Chaddah, Physica C **227**, 176 (1994).
[18] A. M. Campbell and J. E. Evetts, Adv. Phys. **21**, 199 (1972).
[19] D. G. Walmsley, J. Phys. F **2**, 510 (1972).
[20] J. R. Clem, Phys. Rev. B **26**, 2463 (1982).
[21] J. R. Clem and A. Pérez-González, Phys. Rev. B **30**, 5041 (1984).
[22] A. Pérez-González and J. R. Clem, Phys. Rev. B **31**, 7048 (1985).
[23] A. Pérez-González and J. R. Clem, J. Appl. Phys. **58**, 4326 (1985).
[24] J. R. Clem and A. Pérez-González, Phys. Rev. B **33**, 1601 (1986).
[25] A. Pérez-González and J. R. Clem, Phys. Rev. B **43**, 7792 (1991).
[26] J. R. Cave and M. A. R. LeBlanc, J. Appl. Phys. **53**, 1631 (1982).
[27] R. Boyer and M. A. R. LeBlanc, Solid State Commun. **24**, 261 (1977).
[28] R. Boyer, G. Fillion, and M. A. R. LeBlanc, J. Appl. Phys. **51**, 1692 (1980).
[29] M. A. R. LeBlanc and J. P. Lorrain, J. Appl. Phys. **55**, 4035 (1984).
[30] M. A. R. LeBlanc, Cryogenics **32**, 813 (1992).
[31] G. Gandolfini, M.Sc. thesis, University of Ottawa, 1990.
[32] L. Ji, M. S. Rzchowski, N. Anand, and M. Tinkham, Phys. Rev. B **47**, 470 (1993).
[33] L. Krusin-Elbaum, A. P. Malozemoff, D. C. Cronemeyer, F. Holtzberg, J. R. Clem, and Z. Hao, J. Appl. Phys. **67**, 4670 (1990).
[34] J. R. Clem and Z. Hao, Phys. Rev. B **48**, 13 774 (1993).
[35] L. Krusin-Elbaum, A. P. Malozemoff, Y. Yeshurun, D. C. Cronemeyer, and F. Holtzberg, Physica C **153-155**, 1469 (1988).
[36] J. Jung, M. A.-K. Mohamed, I. Isaac, and L. Friedrich, Phys. Rev. B **49**, 12 188 (1994).